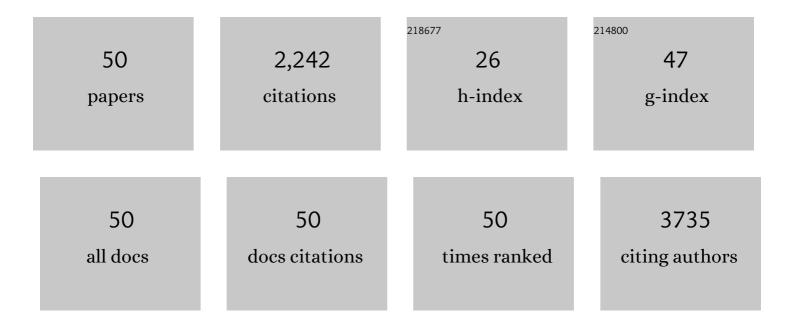
Jun Liu

List of Publications by Year in descending order

Source: https://exaly.com/author-pdf/8551033/publications.pdf Version: 2024-02-01



Тим Гил

#	Article	IF	CITATIONS
1	Bi SPR-Promoted Z-Scheme Bi ₂ MoO ₆ /CdS-Diethylenetriamine Composite with Effectively Enhanced Visible Light Photocatalytic Hydrogen Evolution Activity and Stability. ACS Sustainable Chemistry and Engineering, 2018, 6, 696-706.	6.7	240
2	The formation of onion-like carbon-encapsulated cobalt carbide core/shell nanoparticles by the laser ablation of metallic cobalt in acetone. Carbon, 2013, 55, 108-115.	10.3	119
3	Highly Dispersed Ultrafine Pt Nanoparticles on Reduced Graphene Oxide Nanosheets: In Situ Sacrificial Template Synthesis and Superior Electrocatalytic Performance for Methanol Oxidation. ACS Applied Materials & Interfaces, 2015, 7, 22935-22940.	8.0	107
4	Highly oriented Ge-doped hematite nanosheet arrays for photoelectrochemical water oxidation. Nano Energy, 2014, 9, 282-290.	16.0	104
5	Recent Advances in Surfactantâ€Free, Surfaceâ€Charged, and Defectâ€Rich Catalysts Developed by Laser Ablation and Processing in Liquids. ChemNanoMat, 2017, 3, 512-533.	2.8	103
6	Fe–N-Doped Mesoporous Carbon with Dual Active Sites Loaded on Reduced Graphene Oxides for Efficient Oxygen Reduction Catalysts. ACS Applied Materials & Interfaces, 2018, 10, 2423-2429.	8.0	95
7	Construction of PdO–Pd interfaces assisted by laser irradiation for enhanced electrocatalytic N ₂ reduction reaction. Journal of Materials Chemistry A, 2019, 7, 12627-12634.	10.3	86
8	Carbon-Encapsulated Metal/Metal Carbide/Metal Oxide Core–Shell Nanostructures Generated by Laser Ablation of Metals in Organic Solvents. ACS Applied Nano Materials, 2019, 2, 28-39.	5.0	86
9	Facet-Dependent Selective Adsorption of Mn-Doped α-Fe ₂ O ₃ Nanocrystals toward Heavy-Metal Ions. Chemistry of Materials, 2017, 29, 10198-10205.	6.7	82
10	General Strategy for Doping Impurities (Ge, Si, Mn, Sn, Ti) in Hematite Nanocrystals. Journal of Physical Chemistry C, 2012, 116, 4986-4992.	3.1	75
11	A general strategy toward transition metal carbide/carbon core/shell nanospheres and their application for supercapacitor electrode. Carbon, 2016, 100, 590-599.	10.3	75
12	Co-doped Ni hydroxide and oxide nanosheet networks: laser-assisted synthesis, effective doping, and ultrahigh pseudocapacitor performance. Journal of Materials Chemistry A, 2016, 4, 10609-10617.	10.3	73
13	A novel reduction approach to fabricate quantum-sized SnO2-conjugated reduced graphene oxide nanocomposites as non-enzymatic glucose sensors. Physical Chemistry Chemical Physics, 2014, 16, 8801.	2.8	61
14	Pure Ni nanocrystallines anchored on rGO present ultrahigh electrocatalytic activity and stability in methanol oxidation. Chemical Communications, 2018, 54, 1563-1566.	4.1	60
15	MoS2 nanosheets decorated with ultrafine Co3O4 nanoparticles for high-performance electrochemical capacitors. Electrochimica Acta, 2015, 182, 376-382.	5.2	53
16	In situ growth of lamellar ZnTiO3 nanosheets on TiO2 tubular array with enhanced photocatalytic activity. Physical Chemistry Chemical Physics, 2013, 15, 20203.	2.8	49
17	Ge-doped hematite nanosheets with tunable doping level, structure and improved photoelectrochemical performance. Nano Energy, 2013, 2, 328-336.	16.0	49
18	Spontaneous Growth and Chemical Reduction Ability of Ge Nanoparticles. Scientific Reports, 2013, 3, .	3.3	48

Jun Liu

#	Article	IF	CITATIONS
19	Reduced graphene oxide anchored magnetic ZnFe ₂ O ₄ nanoparticles with enhanced visible-light photocatalytic activity. RSC Advances, 2015, 5, 9069-9074.	3.6	48
20	Photo-excited in situ loading of Pt clusters onto rGO immobilized SnO2 with excellent catalytic performance toward methanol oxidation. Nano Energy, 2016, 26, 699-707.	16.0	48
21	Ultrafine copper nanoparticles anchored on reduced graphene oxide present excellent catalytic performance toward 4-nitrophenol reduction. Journal of Colloid and Interface Science, 2020, 566, 265-270.	9.4	42
22	Silicon-doped hematite nanosheets with superlattice structure. Chemical Communications, 2011, 47, 8040.	4.1	34
23	Ni ³⁺ doped cobalt–nickel layered double hydroxides as high-performance electrode materials for supercapacitors. RSC Advances, 2017, 7, 49010-49014.	3.6	34
24	Understanding the Solvent Molecules Induced Spontaneous Growth of Uncapped Tellurium Nanoparticles. Scientific Reports, 2016, 6, 32631.	3.3	31
25	Layered mesoporous Mg(OH) ₂ /GO nanosheet composite for efficient removal of water contaminants. RSC Advances, 2016, 6, 26977-26983.	3.6	31
26	S,N dual-doped carbon nanotubes as substrate to enhance the methanol oxidation performance of NiO nanoparticles. Carbon, 2019, 152, 114-119.	10.3	29
27	Encapsulation of Co-based nanoparticle in N-doped graphitic carbon for efficient oxygen reduction reaction. Carbon, 2020, 156, 31-37.	10.3	27
28	Strong Fe3+-O(H)-Pt Interfacial Interaction Induced Excellent Stability of Pt/NiFe-LDH/rGO Electrocatalysts. Scientific Reports, 2018, 8, 1359.	3.3	26
29	Oxygen Defects Induce Strongly Coupled Pt/Metal Oxides/rGO Nanocomposites for Methanol Oxidation Reaction. ACS Applied Energy Materials, 2019, 2, 5577-5583.	5.1	26
30	Laser irradiation-induced Au–ZnO nanospheres with enhanced sensitivity and stability for ethanol sensing. Physical Chemistry Chemical Physics, 2016, 18, 22503-22508.	2.8	24
31	Grafting BiOCl nanosheets onto TiO2 tubular arrays to form a hierarchical structure with improved photocatalytic performance. RSC Advances, 2013, 3, 19064.	3.6	23
32	Paramagnetic CuS hollow nanoflowers for <i>T</i> ₂ -FLAIR magnetic resonance imaging-guided thermochemotherapy of cancer. Biomaterials Science, 2019, 7, 409-418.	5.4	23
33	Two-Dimensional IV–V Monolayers with Highly Anisotropic Carrier Mobility and Electric Transport Properties. Journal of Physical Chemistry Letters, 2021, 12, 1058-1065.	4.6	23
34	Simultaneous doping and growth of Sn-doped hematite nanocrystalline films with improved photoelectrochemical performance. RSC Advances, 2014, 4, 63408-63413.	3.6	20
35	Highly dispersed Au nanoparticles decorated WO3 nanoplatelets: Laser-assisted synthesis and superior performance for detecting ethanol vapor. Journal of Colloid and Interface Science, 2018, 514, 165-171.	9.4	20
36	Laser ablation in liquids for the assembly of Se@Au chain-oligomers with long-term stability for photothermal inhibition of tumor cells. Journal of Colloid and Interface Science, 2020, 566, 284-295.	9.4	19

Jun Liu

#	Article	IF	CITATIONS
37	Laserâ€Irradiationâ€Induced Melting and Reduction Reaction for the Formation of Ptâ€Based Bimetallic Alloy Particles in Liquids. ChemPhysChem, 2017, 18, 1133-1139.	2.1	17
38	Structural and electrochemical evaluation of a TiO ₂ –graphene oxide based sandwich structure for lithium-ion battery anodes. RSC Advances, 2015, 5, 45038-45043.	3.6	15
39	Coexistence of resistance switching and negative differential resistance in the α-Fe ₂ O ₃ nanorod film. Physical Chemistry Chemical Physics, 2016, 18, 17440-17445.	2.8	15
40	Pressure induced semiconductor-metallic transition of selenium nanoribbons generated by laser ablation in liquids. Applied Surface Science, 2019, 473, 564-570.	6.1	15
41	Stability evolution of ultrafine Ag nanoparticles prepared by laser ablation in liquids. Journal of Colloid and Interface Science, 2021, 585, 444-451.	9.4	15
42	Defect-Modified Ultrathin BiOX (X = Cl, Br) Nanosheets Via a Top–Down Approach with Effective Visible-Light Photocatalytic Degradation. Journal of Physical Chemistry C, 2021, 125, 18630-18639.	3.1	15
43	In-situ reactive loading of platinum onto tin oxide nanocrystals with superior catalytic performance for hydrogenation of 4-nitrophenol. Applied Surface Science, 2019, 471, 469-474.	6.1	12
44	Ultrafine nanoparticles conglomerated α-Fe2O3 nanospheres with excellent gas-sensing performance to ethanol molecules. Materials Letters, 2018, 211, 239-242.	2.6	11
45	Laser-synthesized graphite carbon encased gold nanoparticles with specific reaction channels for efficient oxygen reduction. Journal of Colloid and Interface Science, 2020, 563, 74-80.	9.4	10
46	Monodispersed carbon nanodots spontaneously separated from combustion soot with excitation-independent photoluminescence. RSC Advances, 2016, 6, 8456-8460.	3.6	8
47	Solvent molecules dominated phase transition of amorphous Se colloids probed by in-situ Raman spectroscopy. Applied Surface Science, 2019, 466, 1000-1006.	6.1	5
48	Simultaneous Cu doping and growth of TiO2 nanocrystalline array film as a glucose biosensor. RSC Advances, 2016, 6, 78219-78224.	3.6	4
49	Construction of Pd/BiOCl Catalyst for Highlyâ€selective Synthesis of Benzoin Ethyl Ether by Chlorine Promoted Coupling Reaction. ChemCatChem, 2019, 11, 2676-2682.	3.7	4
50	Gold-Modified Mo ₂ C Nanoparticles Supported on Nitrogen-Doped Carbon Nanotubes for Electrochemical Nitrogen Fixation. ACS Applied Nano Materials, 2022, 5, 7382-7391.	5.0	3